Crystal Structure of Lamellar Paraffin Eutectics

Douglas L. Dorset

Electron Diffraction Department, Medical Foundation of Buffalo, Inc., Buffalo, New York 14203. *Received February 17, 1986*

ABSTRACT: Electron diffraction and high-resolution, low-dose electron microscopy are used to determine the structure of the two-crystal phase of fractionated binary paraffin mixtures indicated in phase diagrams constructed from differential scanning calorimetric measurements. The pure even-chain paraffins used to form these binary mixtures all crystallize as the orthorhombic polymorph. When the chain length difference for components of the mixture is six methylene units, e.g., n-$C_{30}H_{62}$/n-$C_{36}H_{74}$, a solid solution is formed from the melt which slowly fractionates into a lamellar superlattice. In this superlattice, the lamellae, which presumably are each composed of a single paraffin species, can maintain crystallographic contact with lamellae of the other component across identical methyl end planes. When there is a ten methylene unit chain length difference, e.g., n-$C_{30}H_{62}$/n-$C_{40}H_{82}$, no metastable solid solution is found, since the phase diagram from subsequently cooled and reheated specimens shows this to be a stable eutectic between two immiscible components. For rapidly cooled melts a superlattice structure is also found for the eutectic mixture, which is often in crystallographic contact with domains of the pure n-$C_{40}H_{82}$ component. For neither binary system can the fractionated mixture in the eutectic be described as "mechanical".

Introduction

For a broad spectrum of natural linear-chain materials, the occurrence of polydisperse aggregates is much more common than the existence of pure compounds. Linear alkanes from petroleum, for example, when purified into crystalline wax fractions with narrow melting ranges nevertheless remain polydisperse.[1] Linear polymers such as polyethylene almost always exist as a distribution of molecular weight components and, depending upon the mode of crystallization,[2] can retain a wide range of molecular weights in the chain-folded lamellar crystal habit. Biological lipids are also polydisperse, with acyl chain segments regulated by diet but also the requirements of an individual organelle.[3] In the cell membrane, the admixture of acyl chain species seems to help regulate its phase behavior,[4] which may be useful in processes such as cell fusion. Acyl chain mixtures are also important for the fluidization of neutral lipids such as cholesteryl esters,[5,6] and their phase separation may contribute to pathological states, e.g., atherosclerotic plaque.[6]

The stability of a polydisperse linear-chain aggregate lies in its ability to form solid solutions. For n-paraffins such behavior has been studied often by calorimetric and powder X-ray diffraction techniques, essentially as reviewed in 1960 by Mnyukh.[7] Kitaigorodskii[8] has used such data from molecular crystals to postulate general structural rules for the existence of solid solutions; i.e., the molecular sizes and shapes of the two components must not be too dissimilar and the symmetry of the "host" crystal (solvent) cannot be raised by the "guest" impurity (solute). The size criterion can be evaluated with a parameter of geometrical similarity, $\epsilon = 1 - \Gamma/r$, where r and Γ respectively specify the van der Waals volumes of overlapping and nonoverlapping regions for the components of the binary mixture.[9]

Matching of solute and solvent components in a binary mixture thus minimizes the void volume found in an aggregate of dissimilar species. For linear molecules, the positional substitution allowed for spherical molecules is supplemented by a configurational component (hence the generation of averaged pseudosymmetry in a mixed lattice) as well as a conformational freedom (e.g., the production of point defects in the form of gauche–trans–gauche^{-1} "kinks").[9] Symmetry effects are exemplified by the continuous solubility of an odd-chain paraffin in an even-chain paraffin and also the translational freedom of the smaller chain component when both ingredients have the same molecular and crystal symmetry. Conformational freedom is found in the "quasi-binary system" of a pure paraffin heated near its chain rotor transition for which the point defects, as well as induced void spaces at chain ends, are stabilized in the averaged crystal lattice.[10] When conformational influences are least important, the boundary conditions for continuous solid solution has been stated empirically to be[11]

$$C_N^{max} = 1.244C_N^{min} - 0.411$$

where C_N^{max} and C_N^{min} are respective chain lengths in the binary mixture.

Recently,[10,12–14] quantitative electron crystallographic techniques (i.e., electron diffraction structure analysis and/or high-resolution lattice imaging at low electron beam doses) have been very successful for the characterization of imperfect paraffin crystal lattices because data can be collected from single microcrystals. In an attempt to understand the type of lattice instabilities important for the induction of chain fractionation and also to elucidate the chain packing of a eutectic mixture, such studies have been continued for binary systems near and beyond the chain length boundary condition stated above. In this paper we present the structure of the fractionated chain aggregate formed after the mixture has approached equilibrium at room temperature.

Table I
Summary of Data for Pure Paraffins

paraffin	mp (peak), °C	measd lamellar spacing, Å	obsd major 0kl reflections
n-$C_{30}H_{62}$	66.0	41.00 ± 0.43	0,0,62, 0,0,64 0,1,30, 0,1,32
n-$C_{36}H_{74}$	75.7	48.61 ± 0.16	0,0,74, 0,0,76 0,1,36, 0,1,38
n-$C_{40}H_{82}$	81.5	54.03 ± 0.67	0,0,82, 0,0,84 0,1,40, 0,1,42

Materials and Methods

Crystallization of n-Paraffins. The three even-chain n-paraffins used in this study, i.e., n-triacontane (n-$C_{30}H_{62}$), n-hexatriacontane (n-$C_{36}H_{74}$) (both >99% purity from Supelco Inc., Bellefonte, PA), and n-tetracontane (n-$C_{40}H_{82}$) (Pfaltz and Bauer Inc., Stamford, CT; purity unspecified), have been shown by electron diffraction studies of solution-crystallized and epitaxially crystallized samples to be isostructural[15,16] (also unpublished data); i.e., they all crystallize as the orthorhombic structure determined by Teare[17] (see Figure 1). The space group is $Pca2_1$, with a = 7.42 Å, b = 4.96 Å, and, as discussed in a review of the homologue structures,[18] c = (2.540n + 3.693) Å, where n is the number of carbons in the alkane chain. Physical data for these paraffins

0024-9297/86/2219-2965$01.50/0

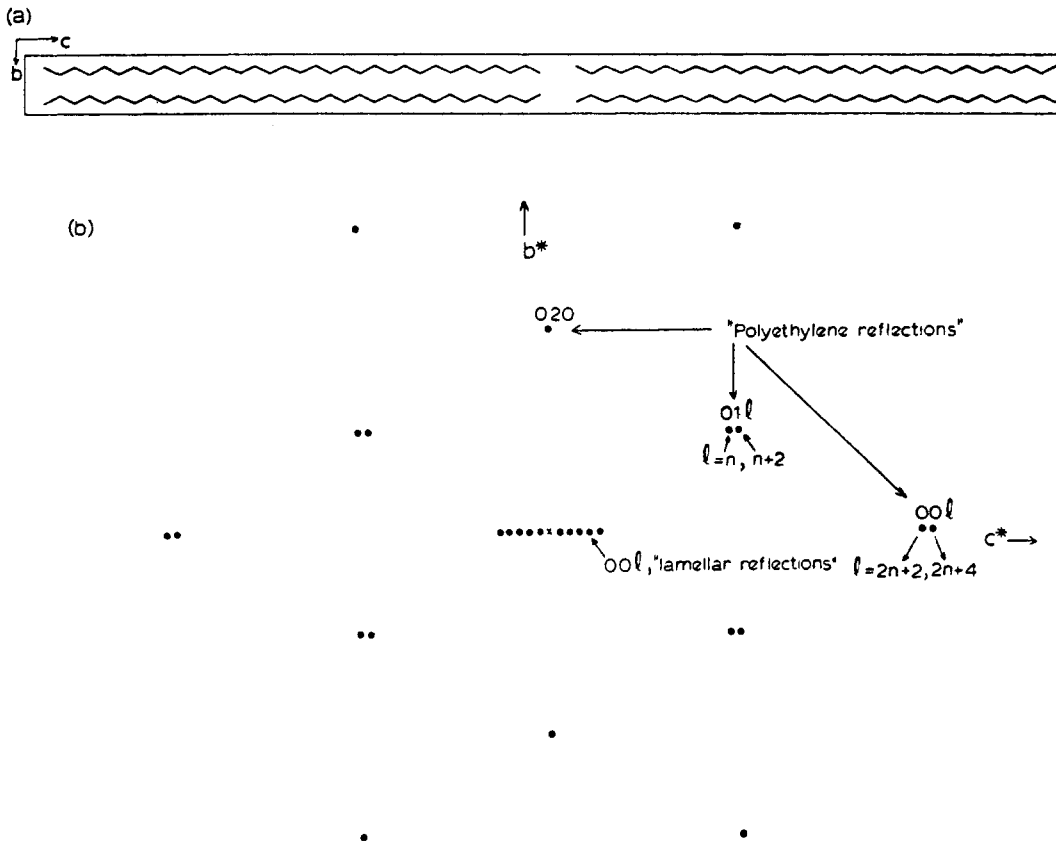

Figure 1. (a) Crystal structure of an even-chain paraffin in the orthorhombic structure, (100) projection. The methylene subcell is $O_{\perp}$.[37] (b) A representative $0kl$ electron diffraction pattern schematized to show the major features. The most intense reflections are due to the Fourier transform of the zigzag chain or "polyethylene" portion of the structure. In addition to the (020) reflection, which is due to the side-to-side packing of the chains, the intense $01l$ and $00l$ peaks are indexed according to the chain length n for the paraffin C_nH_{2n+2}: $(01l)$, $l = n, n + 2$; $(00l)$, $l = 2n + 2, 2n + 4$. The inner $(00l)$ reflections are due to the lamellar repeat of the paraffin layers and, due to the unit cell symmetry (see text), have even index. As found from earlier studies on heated crystals[11] or stable solid solutions,[12] the resolution of these reflections is dependent on the perfection of the lamellar repeat, which can be diminished by introduction of void spaces at the interlamellar interfaces.

are given in Table I. As with the binary mixtures used to form continuous solid solutions,[12] appropriate weight fractions of two compounds were melted and cooled repeatedly in aluminum pans, and a piece of the fused mass was then sealed in an aluminum crucible for differential scanning calorimetric measurement of melting points.

For studies in the electron microscope, samples were epitaxially crystallized on benzoic acid by a technique similar to that described by Wittmann et al.[19] A small piece of the fused sample (representing the same mole fraction as used for calorimetric measurements) was dissolved in hot light petroleum, and the solution was spread on a freshly cleaved mica sheet and allowed to evaporate. Carbon-film-covered electron microscope grids were then placed on regions containing crystallized paraffin, and a larger amount of crystalline benzoic acid was sprinkled around these grids. The other half of the mica sheet was placed over this surface, and the sandwich was moved back and forth on a temperature gradient to cause comelting and recrystallization of the benzoic acid/paraffin mixture. The cooled sandwich was mechanically separated, and the benzoic acid was sublimed away in a vacuum coater, leaving epitaxially oriented paraffin mixtures on the electron microscope grid surfaces.

Differential Scanning Calorimetry. Qualitative differential scanning calorimetric determinations were made with a Mettler FP-800 thermosystem using a scan rate of 2 or 5 °C/min. For each sample an initial heating scan was followed by a cooling scan and then a second heating scan (to evaluate the reproducibility of the melting behavior). (A correction factor for rapid cooling or heating of the specimen was determined to adjust transition temperatures for instrumental or kinetic thermal shifts.) Since the transition behavior of such fractionated systems is more complicated than that for solid solutions, peak maxima positions are plotted in the phase diagrams[20] given here rather than the onset melting temperature given in previous studies.[12] Examples of representative DSC scans are shown in Figure 2. The phase transitions in the DSC scans for the two lower molecular weight components used in the study are typical of paraffins initially packed in the orthorhombic polymorphic crystal form since only two endotherms are found. These endotherms respectively represent the orthorhombic-to-hexagonal and hexagonal-to-melt transitions.[16] The paraffin n-$C_{40}H_{82}$ only undergoes an orthorhombic-to-liquid transition.[16] No evidence is found in any case for the monoclinic polymorph described by Shearer and Vand.[21] The phase transitions have also been characterized by electron diffraction measurements on solution-crystallized specimens using a heating stage in the electron microscope[10] (also unpublished data).

Electron Diffraction and Microscopy. Selected-area electron diffraction experiments were carried out at 100 kV on a JEOL JEM-100B electron microscope using low incident beam intensity and fast photographic film to minimize radiation damage to the specimen, as often described.[22] The diameter of the selected area was approximately 10 μm. When required, the specimens can be heated in the electron microscope with the Gatan 626 stage used in previous studies of phase transitions.[10] Electron diffraction spacings were calibrated with gold Debye–Scherrer diagrams. Densitometry of diffraction patterns utilized a Joyce-Loebl Mk IIIC flat-bed instrument. Lattice imaging experiments were carried out with similarly low incident beam illumination at an instrumental magnification of 20000×. The procedure, developed by Fryer,[23] requires an initial correction of the microscope objective lens for astigmatism at a much higher magnification (>100000×). At a low electron beam current, the sample is translated in the selected-area diffraction mode until a suitably symmetric diffraction pattern is found. A slight translation of the specimen away from this position is required to permit focusing on a reasonably thin crystal edge nearby. After the desired crystal is found again by electron diffraction, the beam is deflected away from

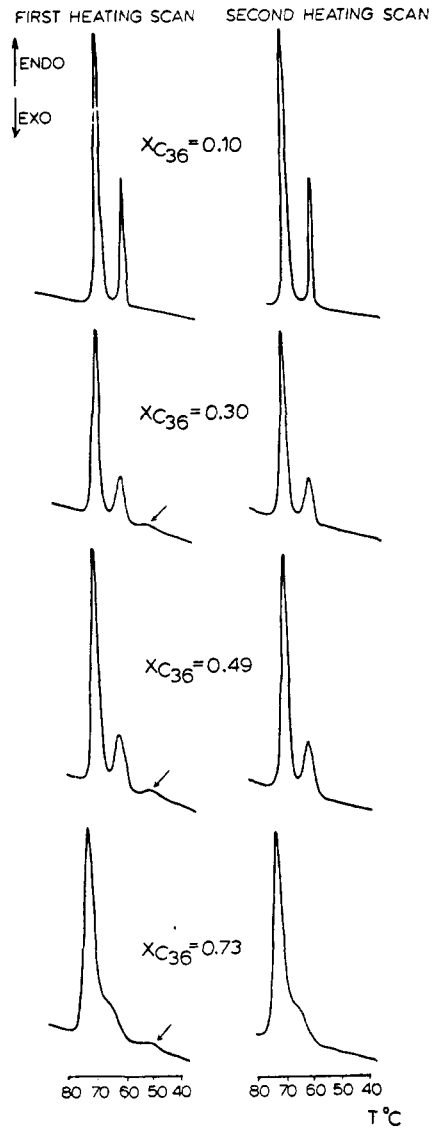

Figure 2. DSC scans of representative binary mixtures of n-$C_{30}H_{62}$ with n-$C_{36}H_{74}$ that had been crystallized from the melt and allowed to equilibrate for several days at room temperature (scan rate: 5 °C/min). Note that a peak near 51 °C disappears when the sample is cooled and reheated. This denotes metastable behavior and, as evidenced from electron diffraction data (see text), a solid solution between the two components is formed first from the cooled melt, which subsequently fractionates.

the specimen with deliberately misaligned "dark-field" controls (deflector coils above the specimen). The microscope lenses are again placed in the imaging configuration and a series of three micrographs is recorded at respectively greater values of underfocus, taking care that the sample is illuminated only during these exposures. After this photographic series, the integrity of the specimen is verified by electron diffraction resolution. For both electron diffraction and microscopy, Kodak DEF-5 X-ray film is used to record the exposures.

Computations. Model kinematical structure factor calculations were carried out with a computer program (provided with the multislice dynamical calculation package obtained from the Arizona State University Facility for High Resolution Electron Microscopy) that uses Doyle–Turner[25] electron scattering factors. Except for the appropriate change in scattering factors, these are identical with calculations made in X-ray crystallography;[24] i.e.

$$F(\vec{h}) = \sum_j f_j \exp(2\pi i \vec{h}\cdot\vec{r}_j)$$

Experimental lattice images were digitized (25-μm raster on the image at 20 000× magnification) on a flat-bed Datacopy microdensitometer at the Fritz-Haber-Institut in Berlin and averaged with computer programs in the image-processing system IMAGIC[26] on a VAX 11/780 computer. Appropriate image areas for this averaging were selected after scanning them on a Polaron optical bench and finding regions with suitable optical transforms. With the image-processing software or by use of the optical bench, much smaller image areas can be sampled than the regions selected in the electron microscope for diffraction. After a suitable area of the specimen is scanned with a densitometer to obtain an array of image density values at x,y coordinate points, this image file can be manipulated with various computer programs in IMAGIC that simulate an optical bench. For example, a Fourier transform operation will generate something similar to an optical diffraction pattern, yet allowing crystallographic phase information to be retrieved. If disorder exists in the original image (as evidenced by continuous scatter around the Bragg peaks), then windows can be defined around these diffraction spots to generate a dark-field image to emphasize details of the crystallographic repeat in this so-called "Fourier-peak filtration". If the Bragg peaks are of finite size and contain phase variations, this reverse Fourier transform will highlight crystal defects (e.g., edge dislocations) that appear in the original image.

It must be emphasized that the epitaxially crystallized n-paraffins represent the orthorhombic polymorph identical with the crystal form found in bulk material used for DSC measurements. This fact was established quantitatively through crystal structure analyses with the elecron diffraction intensity data as described elsewhere.[15,16] The $0kl$ diffraction pattern for pure orthorhombic even-chain paraffin crystals is shown schematically in Figure 1 along with a brief explanation of what different parts of this Fourier transform mean in terms of the depicted crystal structure.

Results

DSC Measurements. (a) n-$C_{30}H_{62}$/n-$C_{36}H_{74}$. DSC scans of $(X)n$-$C_{30}H_{62}$ fused with $(1 - X)n$-$C_{36}H_{74}$ (where X denotes mole fraction) were used to construct the phase diagrams in Figure 3. When mixtures are cooled from the melt, it appears that the two components are continuously soluble over all concentrations, as shown in Figure 3a. As with solid solutions studied earlier,[12] the single-phase regions represent the orthorhombic chain packing, the hexagonal premelt phase, and the liquid phase. However, DSC measurements on samples aged for 2 days at room temperature have a different appearance. A new low-temperature peak, which appears at constant position for a wide range of composition (Figures 2 and 3b), denotes eutectic behavior. (Earlier thermal measurements on this binary system merely described the continuous solubility behavior[27] but not the fractionation indicated in Figure 3b.) If the equilibrated specimens are again recrystallized from the melt, then the eutectic isotherm disappears from subsequent DSC heating scans, signifying the reappearance of the metastable solid solution.

(b) n-$C_{30}H_{62}$/n-$C_{40}H_{82}$. Phase diagrams plotted from DSC scans of an n-$C_{30}H_{62}$/n-$C_{40}H_{82}$ composition series reveal a stable eutectic behavior (Figure 4) that is not influenced by aging or reheating. Unlike the previous case, where the eutectic could be formed by fractionation of a solid solution, the components of this binary mixture are totally immiscible. Estimation of the eutectic composition X_1 (where the subscript denotes the lower melting component) from the measured melting points of the pure components T_1 and T_2 and eutectic temperature T_e can be made with the relationship[28]

$$X_1 = (T_2 - T_e)/(T_1 + T_2 - 2T_e)$$

from which the predicted $X_1 = 0.92$ agrees with experimental measurement. Similar phase diagrams also have been found for paraffin mixtures for which the two components have different crystal structures.[7]

Electron Diffraction. (a) n-$C_{30}H_{62}$/n-$C_{36}H_{74}$. Electron diffraction patterns from equilibrated binary mixtures that had been epitaxially crystallized on benzoic

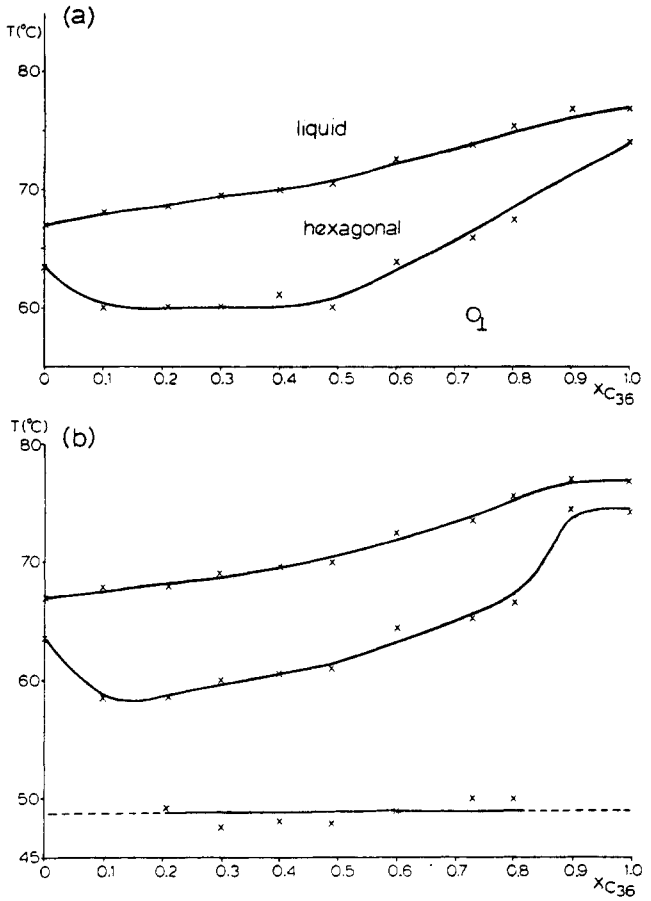

Figure 3. Phase diagrams for n-$C_{30}H_{62}/n$-$C_{36}H_{74}$ constructed from peak temperatures in DSC scans (5 °C/min) (see Figure 2). (a) Phase diagram for samples freshly crystallized from the melt (from heating scans). Its resemblence to phase diagrams published earlier[12] and the electron diffraction data from freshly cooled samples (see text) indicate that continuous solid solutions are formed that represent the $O_\perp$ methylene chain packing[37] of the paraffin at room temperature and the hexagonal chain packing[37] in the premelt phase. (Note that the usual plot[30] of onset and return temperatures for the endotherms in Figure 2 would show the two-phase regions, which are omitted here.) (b) When the samples are allowed to equilibrate at room temperature for several days, an isothermal line near 51 °C appears, which denotes eutectic behavior.[30] The actual position of this first peak appears to be dependent on the time the specimens have to equilibrate; e.g., note the disparity with Figure 2. The extent of the isotherm is not known. Although a eutectic might exist between two solid solutions with limited solubility of one component in the other, we assume in our model calculations that the fractionation is complete.

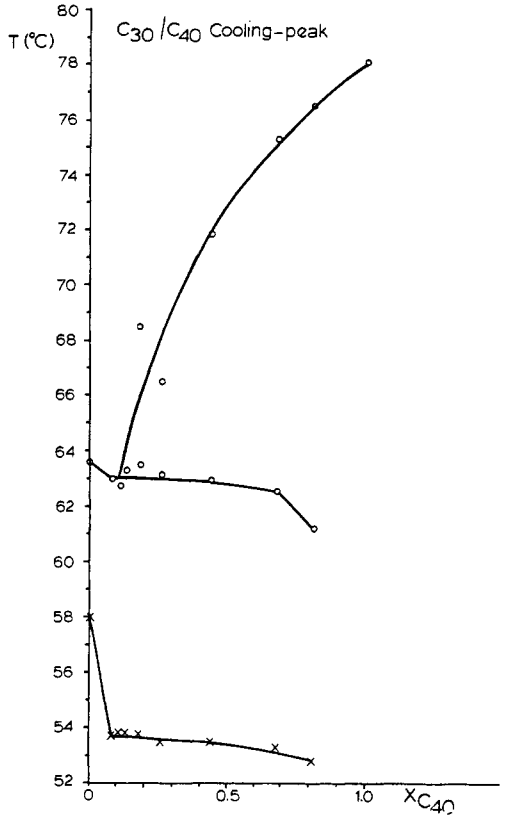

Figure 4. Phase diagram for the binary system n-$C_{30}H_{62}/n$-$C_{40}H_{82}$ constructed from peak values of DSC cooling curves (not shown). No metastable behavior is noted for these mixtures, and the phase diagram clearly indicates a eutectic between two immiscible components.[30]

acid superficially resemble the $0kl$ patterns from pure even-chain n-paraffins or their solid solutions (see Figure 1) except for one salient difference. As shown in Figure 5a,b the $00l$ reciprocal lattice row is comprised of a number of different lamellar spacings, the most intense row of spots having a spacing intermediate to those of the pure components. As shown by the analysis below, it is apparent that these $00l$ diffraction spots are from a superlattice packing of the paraffin components in the binary mixture. The value of the most intense intermediate lamellar spacing is dependent upon the composition of the binary mixture (Figure 6 and Table II). If this lamellar spacing is used to index the major $0kl$ reflections in the diffraction pattern (see Table II), the $01l$ spot indices are odd integers and thus are unlike those expected for the series of even n-paraffins[16] (Table I and Figure 1). The structure, however, is orthorhombic or pseudoorthorhombic. If the superlattice is heated to 64 °C (i.e., within the hexagonal polymorph domain for 2:1 and 1:1 mixtures), only the intense $00l$ spots with an unchanged intermediate spacing remain (Figure 5d), and the sharp intensity falloff of this reciprocal lattice row is similar to that found for stable solid solutions.[12] After the samples cool to room temperature, this reciprocal lattice row *increases* in resolution (Figure 5e) but no additional superlattice spots reappear until the specimens are allowed to equilibrate for 1 or 2 days.

(b) n-$C_{30}H_{62}/n$-$C_{40}H_{82}$. Electron diffraction patterns from epitaxially crystallized n-$C_{30}H_{62}/n$-$C_{40}H_{82}$ mixtures again resemble Figure 5a. The $00l$ row again represents a superlattice that can be indexed in terms of the pure components and an intermediate spacing (Figure 7a). However, unlike the n-$C_{30}H_{62}/n$-$C_{36}H_{74}$ binary system, the most intense reflections in this row are due to the higher molecular weight n-$C_{40}H_{82}$ component. The intermediate spacing is almost constant over all compositions (Figure 6b and Table III). Since the reciprocal lattice row of the pure component row can occasionally be observed to be offset from the superlattice row by a few degrees (Figure 7b), it appears that the higher molecular weight component can separate as a pure phase, as is expected for rapidly cooled melts of the immiscible components (see phase diagram in Figure 4).

Electron Microscopy. (a) n-$C_{30}H_{62}/n$-$C_{36}H_{74}$. Areas of electron micrographs from equilibrated samples selected for image analysis (a 512 × 512 pixel array or approximately (7250 Å)^2) appear to be continuous crystalline regions without obvious grain boundaries. A 1:1 binary mixed-crystal area (Figure 8a) gave a computed Fourier transform (Figure 8b) with a single 45.6-Å spacing. As shown for stable solid solutions,[13] such computed transforms can be used to reproduce the electron diffraction

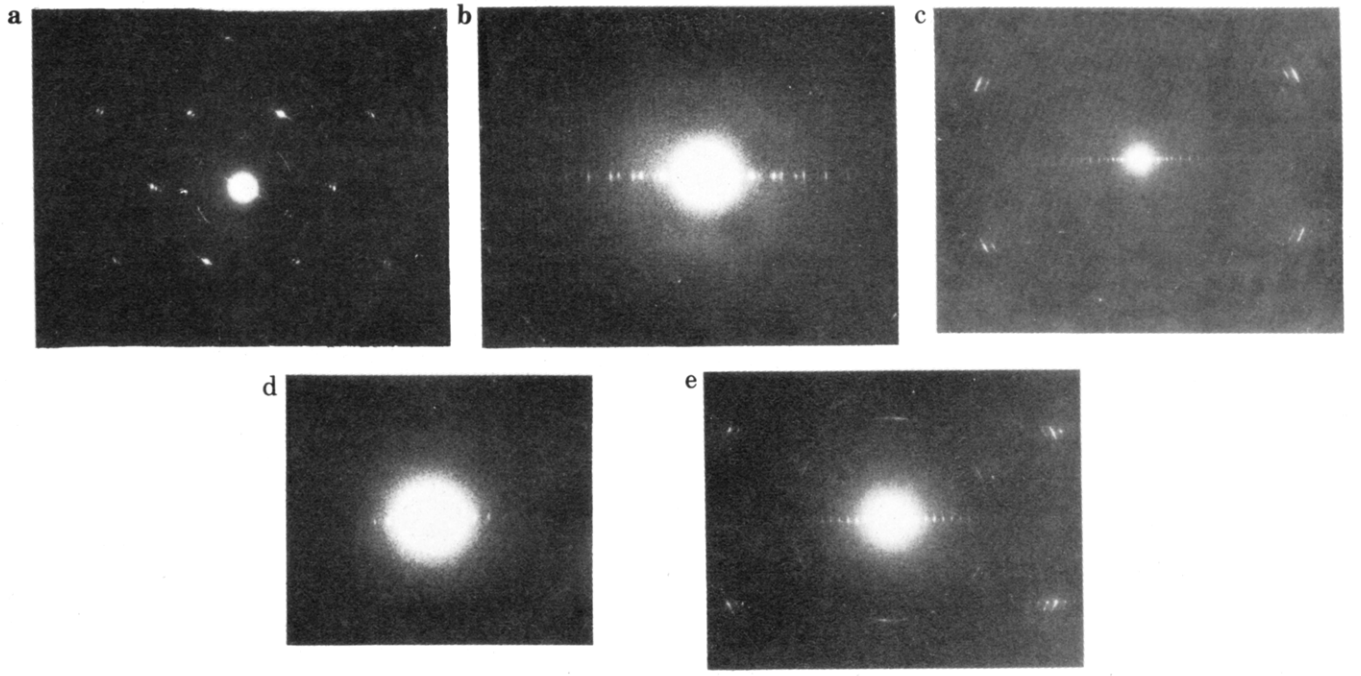

Figure 5. Electron diffraction patterns ($0kl$) from epitaxially crystallized binary mixtures of n-$C_{30}H_{62}$/n-$C_{36}H_{74}$ that had been allowed to equilibrate for several days: (a) 2:1 mixture: note that the $0kl$ pattern superficially resembles those from pure paraffins[15,16] or their solid solutions[12] except that (b) the ($00l$) row is comprised of numerous reflections (Table II), which may denote a superposition of various lamellar spacings or a superlattice (model calculations support the latter thesis). The most intense reflections (see also Figure 6a) indicate a lamellar spacing between the values that would be found for the pure components (Table I). (c) Electron diffraction pattern from a 1:1 equilibrated mixture, again showing superlattice $00l$ spots. When such a sample is heated to 64 °C, only the most intense $00l$ spots remain (d) with the same intermediate spacing. There is no trace of a superlattice. When this a sample is kept at 21 °C for 2 h, the resolution of the $00l$ row improves (e) but no additional superlattice spots reappear until at least 24 h of standing.

Table II
Comparison of Major Reflections for Various Mole Ratios in Crystallized n-$C_{30}H_{62}$/n-$C_{36}H_{74}$ Binary Mixtures

d_{00l}^{obsd},[a] Å			d_{00l}^{calcd},[b] Å			
X_{C36} = 0.20	X_{C36} = 0.41	X_{C36} = 0.66	X_{C36} = 0.25	X_{C36} = 0.33	X_{C36} = 0.50	X_{C36} = 0.66
45.1 w	46.61 s	47.61 s	41.32 s	42.02 s	43.76 s	45.02 s
						27.02 w
22.25 s	22.94 s	22.71 s	20.66 s	21.01 ms	21.89 s	22.52 s
18.22 w	17.23 w			18.01 m	17.50 m	16.89 m
14.81 s	15.27 m	15.38 ms	13.78 ms	14.01 m	14.59 m	15.01 m
12.76 w	12.58 w	12.15 m	12.72 m	12.61 ms	12.50 ms	12.28 ms
11.10 m	11.38 w	11.44 w				11.26 w
9.91 m	9.88 w	9.63 m	9.72 ms	9.70 ms	9.72 s	9.65 s
8.91 m						
8.10 m	8.10 w	7.95 m	7.87 s	7.88 s	7.96 s	7.95 s
	6.88 w	6.81 m	6.61 m		6.73 s	6.75 s

Major $0kl$ Reflections Where Most Intense d_{00l} Determine Indices

obsd	calcd (1:1 model)	obsd	calcd (1:1 model)
0,1,33	0,1,33	0,0,68	0,0,68
0,1,35	0,1,35	0,0,70	0,0,70

[a] From observed lamellar reflections. [b] From model calculations on superlattices.

results plotted in Figure 6a. Calculated dark-field images also are similar in appearance to those from stable solid solutions (Figure 8c); enlargements of these (Figure 8d) emphasize the presence of lamellar terminations (which also are observed for pure paraffins and their solid solutions).[13]

(b) n-$C_{30}H_{62}$/n-$C_{40}H_{82}$. Images from 2:1 and 1:1 binary mixtures (Figures 9a and 10a) were sampled with the same area size used for the binary mixture in Figure 8. Computed Fourier transforms of both image domains (Figures 9b and 10b) contain two separate lattice spacings—one from the pure component and the intermediate spacing, as seen in electron diffraction experiments. When the two lattice spacings are selected separately for image averaging via Fourier peak filtration, the respective dark-field images from the continuous crystal area are complementary to each other (compare Figures 9c,d and also Figures 10c,d), highlighting areas that contain either the eutectic crystalline mixture or the pure component. The boundaries between these separate regions are fairly sharp (allowing for image contrast changes due to local bending) and, as also indicated by the electron diffraction data, are thus crystallographically aligned to each other. Note also that the relative areas of each component in each mixture are roughly dependent on the mole ratio of the pure components in the mixture.

Structure Analysis

From the data presented above, it is apparent that the two binary systems in this study have both distinguishing

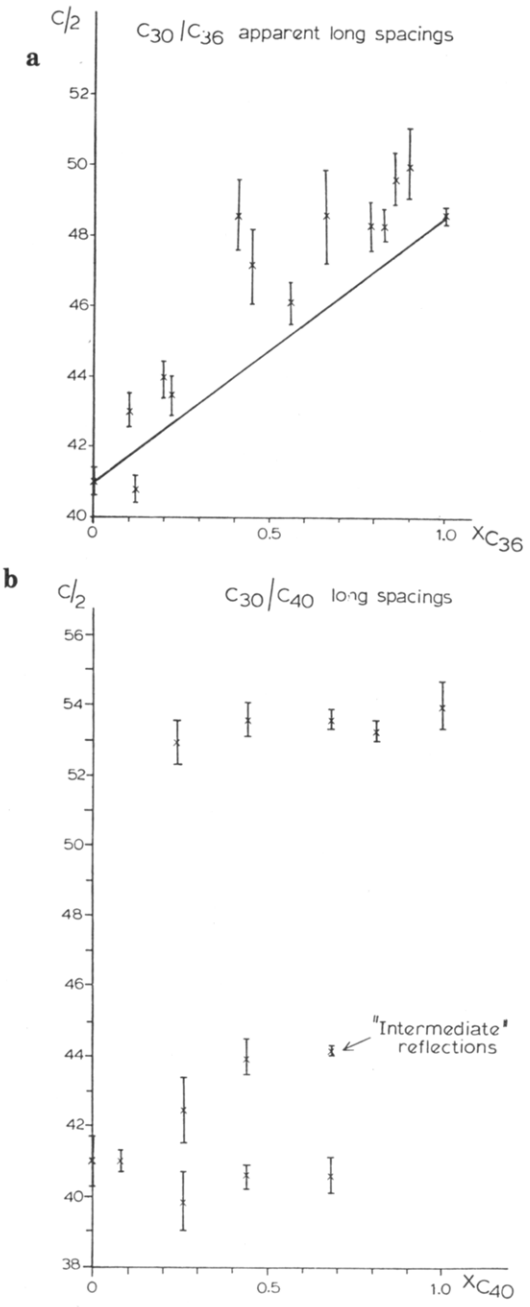

Figure 6. Plots of lamellar spacings from experimental $0kl$ electron diffraction patterns for different compositions of the two binary paraffin series. (a) Equilibrated n-$C_{30}H_{62}$/n-$C_{36}H_{74}$: only the most intense lamellar spacing is plotted here and is shown to resemble similar plots for stable solid solutions. Note that the lamellar spacing values mainly lie above the line drawn from Vegard's law.[9] The "standard deviation" of these values (averaging over numerous mixed crystals) probably indicates local compositional variations in these rapidly cooled samples. (b) Equilibrated n-$C_{30}H_{62}$/n-$C_{40}H_{82}$. Here the most intense lamellar row is due to the higher molecular weight component. The spacings due to the lower molecular weight component and the intermediate superlattice value are also nearly invariant with composition.

and similar features. Either forms a eutectic at equilibrium and crystallizes as a lamellar superlattice. The components with the greater chain length difference are totally immiscible and thus form a stable eutectic. When the chain length difference is smaller, the system is metastable, initially forming a solid solution from the cooled melt which slowly fractionates. From the phase diagram in Figure 3 it is not clear whether limited solubility remains between the components after fractionation, because the extent of the isotherm is not determined. In our model calculations

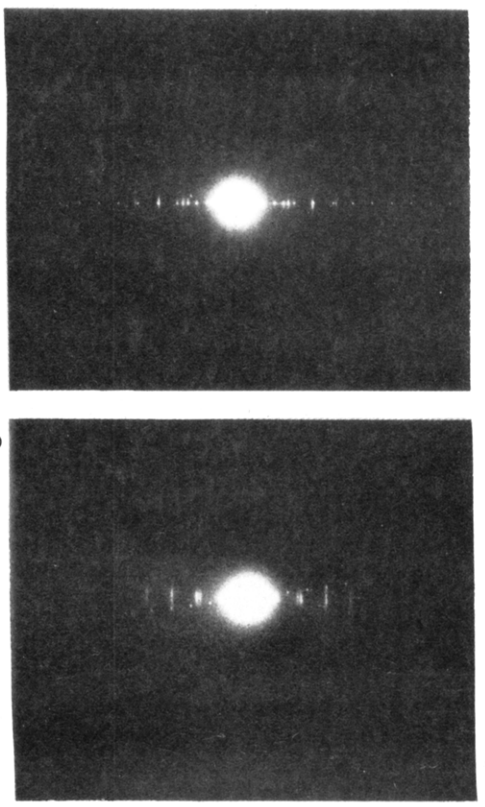

Figure 7. Electron diffraction patterns from epitaxially crystallized n-$C_{30}H_{62}$/n-$C_{40}H_{82}$ mixtures. The $0kl$ pattern for many mixtures superficially resembles Figure 5a and includes (a) a row of $00l$ spots with superlattice spacings. Sometimes (b) the superlattice row is offset a few degrees from a $(00l)$ row from the pure n-$C_{40}H_{82}$ component. (Such domains of the pure component are not found for the n-$C_{30}H_{62}$/n-$C_{36}H_{74}$, system.) A plot of lamellar spacings is given in Figure 6b.

Table III
Comparison of Lamellar Reflections for Various Mole Ratios in Crystallized n-$C_{30}H_{62}$/n-$C_{40}H_{82}$ Binary Mixtures

d_{00l}^{obsd}, [a] Å			d_{00l}^{calcd}, [b] Å
X_{C40} = 0.26	X_{C40} = 0.44	X_{C40} = 0.68	X_{C40} = 0.50
	53.35 w	55.04	
45.05	44.59 s	45.05	46.30 s
27.34	26.92 ms	27.17	30.86 m
21.74	22.30 ms	22.13	23.15 m
20.32	19.85 ms	20.22	
18.12	17.93 ms	18.19	18.52 ms
13.80	13.69 s	13.63	13.23 s
10.80	10.80 ms	10.83	
10.48	10.50 ms		10.29 s
9.06	9.03 m	9.08	9.26 m
7.73	7.71 m	7.74	7.72 m
6.79	6.73 m	6.77	6.61 ms
6.02			
5.84		5.98	5.79 m

[a] From observed reflections. [b] From model superlattice calculation.

below, we assume the fractionation to be complete.

The most interesting feature of both systems is the mixed layer structure in the eutectic, which denotes a crystallographic register of the component lamellar layers in the fractionated mixture. A possible model for such an intimate mixture is the superlattice depicted in Figure 11. In this model, individual lamellae are allowed to retain the layer structure found for a pure even-chain orthorhombic paraffin, i.e., half of the unit cell given by Teare.[17] A second, isostructural, lamella made up of a different chain length component can pack in crystallographic register

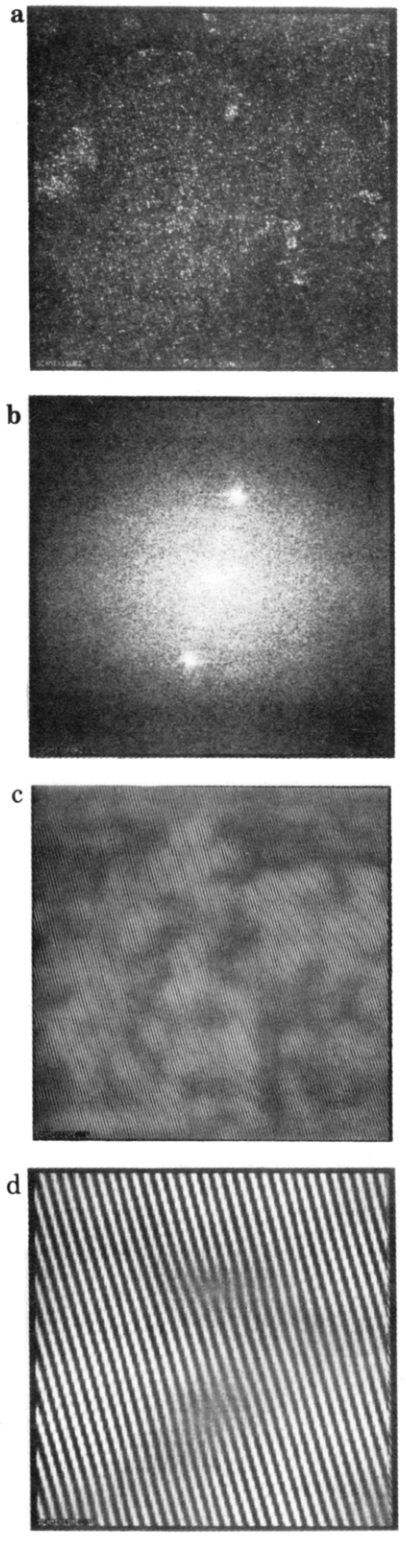

Figure 8. Image analysis of a ca. 1:1 binary mixture of n-$C_{30}H_{62}$ with n-$C_{36}H_{74}$: (a) experimental image; (b) computed Fourier transform (the intense intermediate spacing from the superlattice agrees with electron diffraction data (Figure 5)); (c) image obtained when the diffraction spots in (b) are passed through a mask. (d) Note the presence of lamellar terminations seen also for pure paraffins and their solid solutions[13] in the enlargement of (c). At low magnification the crystal regions used in the image analysis appear to be continuous; i.e., there are no apparent grain boundaries due to phase separation in the equilibrated mixtures.

with the first one since the methyl end plane packings of both layers are identical. Of course, the juxtaposition of two different lamellae will destroy the space group symmetry found for the pure components (see Figure 1).

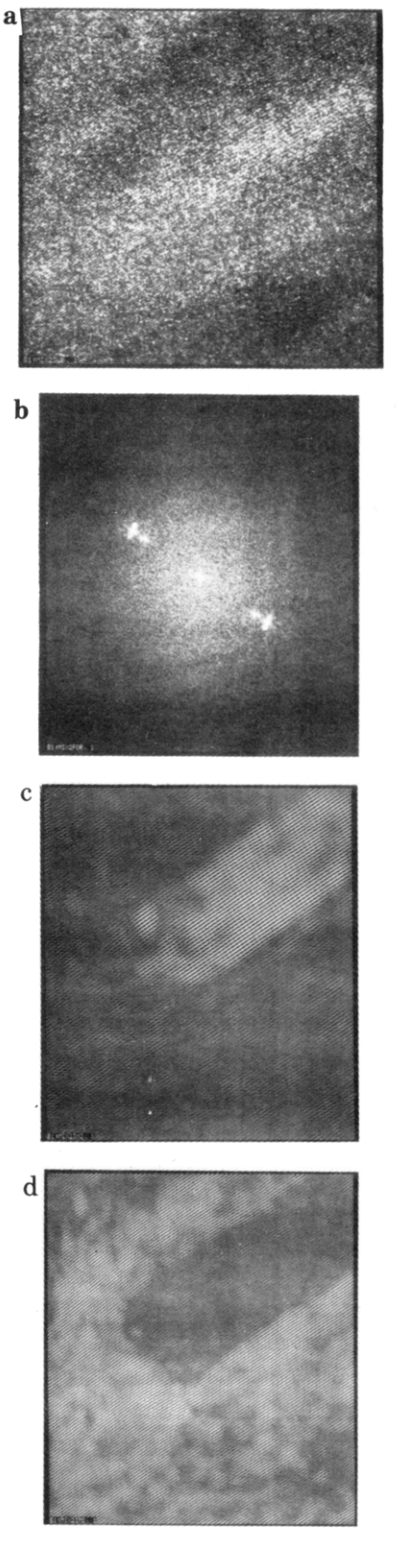

Figure 9. Image analysis of ca. 2:1 mixture of n-$C_{30}H_{62}$/n-$C_{40}H_{82}$ for which the low-magnification crystal image again appears to be continuous. (a) Experimental image that has the computed Fourier transform in (b). This $00l$ row is similar to electron diffraction data (Figure 7) since lamellar spacings due to the eutectic mixture (intermediate spacing) and also the pure n-$C_{40}H_{82}$ component are found. Image reconstruction with respective lattice repeats thus gives complementary dark-field images of domains containing (c) pure n-$C_{40}H_{82}$ component and (d) the eutectic superlattice. It should be pointed out here that separate domains of the mixed crystal lattice image can be isolated on an optical bench if the sampled area is small enough. The resultant optical transforms again are due to either the superlattice or pure n-$C_{40}H_{82}$.

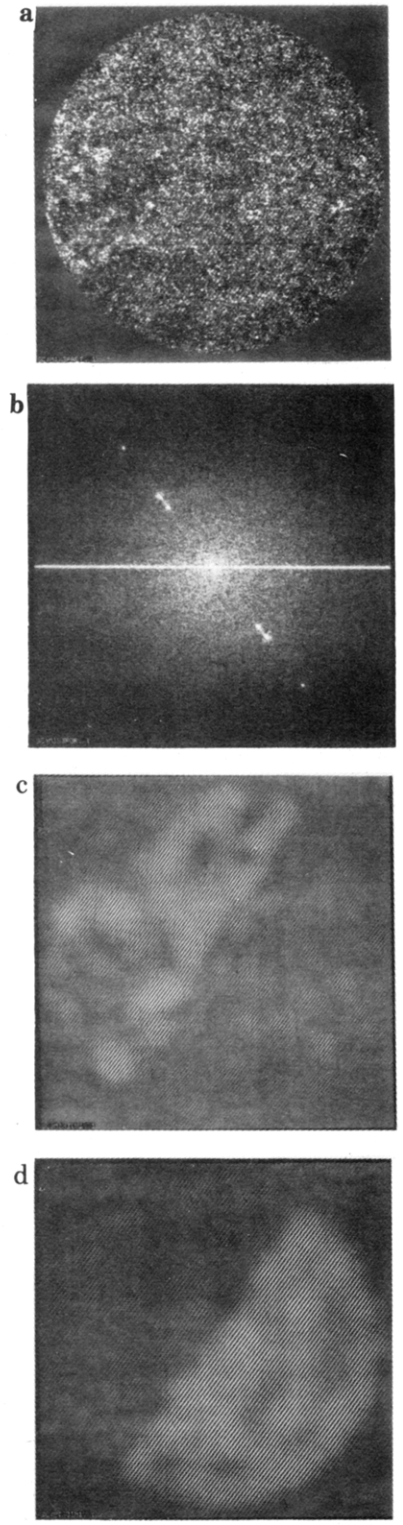

Figure 10. Image analysis of a ca. 1:1 mixture of n-$C_{30}H_{62}$/n-$C_{40}H_{82}$ as in Figure 9: (a) experimental image; (b) its computed Fourier transform; (c) dark-field image formed from the lattice repeat of the higher molecular weight component; (d) dark-field image formed from the lattice repeat of the eutectic superlattice. In both Figure 9 and this figure the boundaries between pure and mixed-crystal phase domains appear to be fairly sharp, especially along the (001) plane (i.e., the striation direction).

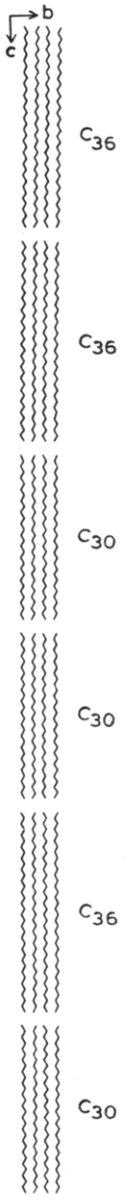

Figure 11. Superlattice model used to explain the experimental results; an alternating n-$C_{30}H_{62}$/n-$C_{36}H_{74}$ structure is shown. Comparison with Figure 1a reveals that the layer packing of the orthorhombic paraffin is maintained but, due to the random occurrence of successive lamellae with differing layer thickness, the space group symmetry is not maintained. Calculation of structure factors with such models (Tables II and III) explains many features of the observed electron diffraction patterns, including the apparent index of major $0kl$ reflections and the positions of $(00l)$ superlattice reflections. The concentration dependence of the latter values is least precise, possibly because of the statistical variations of composition in microareas of the mixed crystals because the samples are rapidly cooled.

Representative superlattice structure models based on Figure 11 but differing only in the respective abundance of individual lamellae, were used to calculate $0kl$ intensities for both the n-$C_{30}H_{62}$/n-$C_{36}H_{74}$ and n-$C_{30}H_{62}$/n-$C_{40}H_{82}$ systems. For a given composition, the ordering of lamellae in the superlattice is not important so long as they are randomly mixed. The indices of the major $0kl$ reflections are accounted for by this calculation (Table II). Moreover, calculated relative intensities and reciprocal spacings of $00l$ reflections also explain their concentration dependence of their observed values for the n-$C_{30}H_{62}$/n-$C_{36}H_{74}$ mixtures. These calculations also explain why reflections with the "intermediate" spacing have the least standard deviation from their expected values at increasing diffraction orders whereas reflection spacings, corresponding to the pure compounds, can deviate significantly from values expected at all orders of either pure component lattice repeat (see Table II). Nevertheless there is not an exact matching of the spacings for comparable values of simu-

lated and experimental mole ratios, even though calculated and observed 00l lattice spacings can be found at nominally different compositions that have a reasonable match in all lattice spacings (Table II). (This discrepancy may be due to the rapid crystallization of this system to produce areas with nonequilibrium concentrations of respective lamellae[29] according to the local concentrations in the original solid solutions (see also Figure 6a).) The expected invariance of the n-$C_{30}H_{62}$/n-$C_{40}H_{82}$ eutectic mixture lattice spacing is indicated by experimental data in Table III, and the reflection positions are in agreement with the calculated 1:1 random superlattice. In this case, however, reflection positions from the higher molecular weight component deviate least from expected values at all orders of the lattice repeat only because n-$C_{40}H_{82}$ also exists at a separate phase (see above and Table III). In every example for both systems, crystal areas sampled for the diffraction or imaging experiments are continuous, as indicated by the lattice image textures, since no grain boundaries of the type seen for aromatic structures[30] are found between domains of mixed-component crystal. This is even true for the mixtures containing domains of pure component.

It might be argued that an alternative structure for the eutectic mixture would be one where pure phase domains for a given component extend over several lamellae. Were this to happen, then the strongest diffraction peaks of lamellar 00l reflections would have spacings corresponding to the pure components instead of the intermediate values found for one example above. These spacings, moreover, should be elongated along c^* due to an average shape transform[31] for the sequestered, narrow domains of pure components—an expectation that also does not correspond to the observed diffraction peak sharpness (Figures 5 and 7).

Discussion

Metastable binary mixtures of n-paraffins have been studied earlier by powder X-ray and thermal techniques. Mazee[32] described the system n-$C_{30}H_{62}$/n-$C_{35}H_{72}$ as one that forms a continuous solid solution or a eutectic of solid solutions. After fused samples were aged for a year, superlattice lines were observed in powder X-ray diagrams. (Although the symmetries of odd and even paraffin components are different, it is now known that the higher energy B polymorph of the odd-chain paraffin can form solid solutions with the orthorhombic even-chain paraffins.[12]) The superlattice structure determined in the present study, which is probably similar to the one detected in Mazee's work, is an optimal packing mode for the eutectic mixture after chain fractionation, both from the standpoint of molecular association and allowing for necessary longitudinal diffusion of chains across the lamellar interfaces when the mixture is heated. That a similar diffusion process may be important for the formation of stable solid solutions has been shown when two pure paraffin crystals of unequal chain length are placed in contact across their (001) faces.[33,34]

It is also apparent that the mechanism for chain fractionation is somewhat complicated. When the n-$C_{30}H_{62}$/n-$C_{36}H_{74}$ mixtures are heated near the "chain rotor" hexagonal phase to induce solid solution formation, the lamellar diffraction data are very similar to those found for stable solid solutions; i.e., there is an attenuated resolution of these reflections due to the production of chain end gaps in the mixed-chain lamellae as described earlier.[12,35] However, the observed increase in diffraction resolution for these reflections for the cooled metastable solid solution before it fractionates is not found in stable solid solutions. This may denote some defect mechanism for minimizing the void volume at the lamellar interfaces. Such a mechanism could be optimally detected by an infrared and Raman study of chains selectively deuterated at specific sites.[36] Clearly, further work is needed to characterize the progress of fractionation in greater detail and also to permit the quantitative determination of crystal structures for the metastable states.

Acknowledgment. This work was supported in part by NSF Grant DMR81-16318 and NIH Grant AM19856. Special thanks are due to Dr. M. van Heel and Prof. E. Zeitler for support in use of computing facilities, image-processing programs, and a densitometer in the Electron Microscopy Department at the Fritz-Haber-Institute of the Max-Planck-Gesellschaft in Berlin/Dahlem. The author also thanks Drs. J. C. Wittmann and J. R. Fryer for helpful discussions and advice in this work.

References and Notes

(1) Chichalki, M.; Jessen, F. W. *Ind. Eng. Chem.* **1967**, *59*(5), 86.
(2) Smith, P.; Manley, R. St. J. *Macromolecules* **1979**, *12*, 483.
(3) Cullis, P. R.; DeKruijff, B.; McGrath, A. E.; Morgan, C. G.; Radda, G. K. In *Structure of Biological Membranes*; Abrahamsson, S., Pascher, I., Eds.; Plenum: New York, 1977; p 389.
(4) Bach, D. In *Biomembrane Structure and Function*; Chapman, D., Ed.; Macmillan: London, 1983; pp 1–41.
(5) Sawzik, P.; Craven, B. M. *Proceedings of the International Conference on Liquid Crystals*, Bangalore, India; Chandrasekhar, S., Ed.; Heyden: Philadelphia, 1980; p 171.
(6) Small, D. M. *Adv. Exptl. Med. Biol.* **1980**, *7*, 55.
(7) Mnyukh, Yu. V. *Zh. Strukt. Khim.* **1960**, *1*, 370.
(8) Kitaigorodskii, A. I. *Organic Chemical Crystallography*; Consultants Bureau: New York, 1961; p 231.
(9) Kitaigorodsky, A. I. *Mixed Crystals*; Springer: Berlin, 1984; p 219.
(10) Dorset, D. L.; Moss, B.; Wittmann, J. C.; Lotz, B. *Proc. Natl. Acad. Sci. U.S.A.* **1984**, *81*, 1913.
(11) Matheson, R. R., Jr.; Smith, P. *Polymer* **1985**, *26*, 288.
(12) Dorset, D. L. *Macromolecules* **1985**, *18*, 2158.
(13) McConnell, C. H.; Fryer, J. R.; Dorset, D. L.; Zemlin, F. *Inst. Phys. Conf. Ser.* **1985**, *78*, 433.
(14) Dorset, D. L. *Inst. Phys. Conf. Ser.* **1985**, *78*, 411.
(15) Moss, B.; Dorset, D. L. *J. Polym. Sci., Polym. Phys. Ed.* **1984**, *22*, 1919.
(16) Dorset, D. L. *J. Polym. Sci., Polym. Phys. Ed.* **1986**, *24*, 79.
(17) Teare, P. W. *Acta Crystallogr.* **1959**, *12*, 294.
(18) Nyburg, S. C.; Potworowski, J. A. *Acta Crystallogr., Sect. B* **1973**, *B29*, 347.
(19) Wittmann, J. C.; Hodge, A. M.; Lotz, B. *J. Polym. Sci., Polym. Phys. Ed.* **1983**, *21*, 2495.
(20) Smith, P.; Pennings, A. J. *Polymer* **1984**, *15*, 413.
(21) Shearer, H. M. M.; Vand, V. *Acta Crystallogr.* **1956**, *9*, 379.
(22) Dorset, D. L. *J. Electron Microsc. Techn.* **1985**, *2*, 89.
(23) Fryer, J. R. *Inst. Phys. Conf. Ser.* **1981**, *61*, 19.
(24) Dunitz, J. D. *X-ray Analysis and the Structure of Organic Molecules*; Cornell University: Ithaca, NY, 1979.
(25) Doyle, P. A.; Turner, P. S. *Acta Crystallogr., Sect. A* **1968**, *A24*, 395.
(26) Heel, M. v.; Keegstra, W. *Ultramicroscopy* **1981**, *7*, 113.
(27) Nechitailo, M. A.; Topchiev, A. V.; Rozenberg, L. M.; Terent'eva, E. M. *Russ. J. Phys. Chem.* (*Engl. Transl.*) **1960**, *34*, 1268.
(28) Hsu, E. C.-H.; Johnson, J. F. *Mol. Cryst. Liq. Cryst.* **1974**, *27*, 95.
(29) Gordon, P. *Principles of Phase Diagrams in Materials Systems*; McGraw-Hill: New York, 1968.
(30) Murata, Y.; Baird, T.; Fryer, J. R. *Nature* (*London*) **1976**, *262*, 721.
(31) Vainshtein, B. K. *Structure Analysis by Electron Diffraction*; Pergamon: Oxford, 1964; p 22.
(32) Mazee, W. M. *Prepr.—Am. Chem. Soc., Div. Pet. Chem.* **1958**, *3*(4), 35.
(33) Ungar, G.; Keller, A. *Colloid Polym. Sci.* **1979**, *257*, 90.
(34) Zerbi, G.; Piazza, R.; Holland-Moritz, K. *Polymer* **1982**, *23*, 1921.
(35) Asbach, G. I.; Geiger, K.; Wilke, W. *Colloid Polym. Sci.* **1979**, *82*, 2811.
(36) Maroncelli, M.; Strauss, H. L.; Snyder, R. G. *J. Am. Chem. Phys.* **1985**, *82*, 2811.
(37) Abrahamsson, S.; Dahlen, B.; Löfgren, H.; Pascher, I. *Prog. Chem. Fats Other Lipids* **1978**, *16*, 125.